An experimental assessment of fracture toughness in novel crimp-free-based composite materials for aerospace applications

Marcello A. Lepore[1] | **Angelo R. Maligno**[1] | **Giacomo Canale**[2] | **Linden Harris**[3]

[1]Institute for Innovation in Sustainable Engineering, University of Derby, Derby, UK

[2]Rolls-Royce plc, Derby, UK

[3]Airbus Operations UK Ltd, Bristol, UK

Correspondence
Marcello A. Lepore, Institute for Innovation in Sustainable Engineering, University of Derby, Derby, UK.
Email: m.lepore@derby.ac.uk

Abstract

In the design of structural composite components for aerospace applications, durability and reliability play a very significant role. To assess the reliability of these material it is essential to carry out robust experimental tests on several specimens and under different loading conditions to allow the determination of fundamental fracture parameters. Fracture toughness, in particular, allows the quantification of the material strength to fracture. This work proposes a study on non-crimp fabric (NCF) together with a two-component epoxy resin. The selected system has been selected based on its suitability to produce aerospace-approved components using resin transfer molding (RTM) process. The fabric adopted is a SAERTEX NCF with very high modulus and strength, whereas the resin is BDP 4294. This work shows the methods, equipment, and results of an experimental campaign carried out to determine the fracture toughness of the manufactured NCF composite material. Finally, to quantify the fracture toughness of the NCF composite material, Mode I, II, Mixed Mode I–II, and translaminar fracture tests were also considered.

KEYWORDS

DCB, ENF, experimental test, mode I, Mixed Mode I–II, translaminar fracture toughness, NCF, RTM

1 | INTRODUCTION

Prepregs represent the selected materials for lightweight structures in the aerospace industry, whereas resin infusion technology is not broadly adopted. NCF composites are preferred as they benefit from highly automated production processes[1] together with the improved damage tolerance capability. Several studies have been conducted to characterize the mechanical properties of NCFs and to identify the damage initiation and propagation.[2–15] For instance, Mode I delamination was investigated by considering the effect of reinforcements through thickness.[16] Experimental and numerical investigations have been employed to analyze Mode II, Mixed mode I–II, and the translaminar fracture toughness were investigated by numerous authors.[17–23] Computational modeling of failure of NCF can be evaluated with reliability by treating each ply in the laminate as a quasi-unidirectional (UD) (QU) composite and by adopting the most appropriate failure criteria. FE codes have been implemented with a wide range of ply failure criteria, and delamination criteria using cohesive zone elements were implemented.[24–28] Although the through-thickness stitching does increase fracture toughness for each blanket, delamination is still likely to occur, due to the presence of resin-rich layers between blankets. In this work,

aerospace-approved NCF textile and two-component epoxy resin have been used to study the fracture strength of the composite specimens.

It is paramount to notice that the innovative resin system has been produced specifically for aeronautical applications. This resin was not commercially available at the time of the testing campaign so, all the resulting experimental data originated from this work can be considered original. This testing campaign has proved that the artifacts resulting from the use of this resin in combination with the selected fabric are suitable to replace current metal structural parts of the landing gears.

Thus, the composite sample has been manufactured via an RTM process. The adopted fabric used is a SAERTEX U-C-298 g/m2-1270mm NCF with a very high modulus and strength, whereas the selected resin is BDP 4294. The selected fabric can be considered UD and virtually wave-free. The UD carbon fibers are the load-bearing reinforcements. The glass fibers present in the fabric are organized in three different directions (90°, −60°, 60°). Glass fibers contribute, together with a through-thickness stitching, to keep the carbon fibers in place during the impregnation process with RTM. The adopted Saertex UD textile has a higher load-bearing capacity than conventional Glass UD fabrics providing up to 20% improvement in tensile strength. Experimental tests were aimed to characterization of fracture toughness behavior of the new material. This experimental campaign is part of the Clean SKY2/ Matrix Project. Experimental tests of Mode I, Mode II, Mixed Mode I–II, and translaminar fracture toughness were performed to determine the fracture toughness of the NCF composite material under different loading conditions. Tests were carried out at room temperatures and in controlled humidity conditions. In previous works, the authors analyzed the behavior of the NCF material under "critical" temperature conditions.[29,30] An experimental campaign was undertaken on composite materials samples with different layups to characterize their behavior at −54°C and at the glass transition temperature (68°C). Composite material samples were also aged for 6 months in an environmental chamber at measured temperature and humidity. The effect of temperature on the overall performance of composite components, especially in aerospace applications, has led to numerous studies aimed to investigate the response to quasi-static loads on carbon fiber reinforced polymers (FRP).[31–33] As far as the experimental tests for the evaluation of the fracture toughness of the NCF composite, these tests were carried out according to ASTM standards. The fracture toughness values have been reported as energy release rate, G. This parameter can be used for numerical simulations in the study of delamination between the ply (e.g., cohesive zone element models).

2 | MATERIALS AND METHODS

2.1 | Materials

2.1.1 | Non-crimped fabric

Aerospace-approved QU fabrics and resin have been selected for RTM process in accordance with European-funded Clean Sky Two MATRIX project requirements. Namely, the U-C-298 g/m^2-1270mm SAERTEX crimp-free fabric with a very high modulus and strength has been selected. The fabric construction has been reported in literature.[29,30]

2.1.2 | Epoxy resin

The approved two-component epoxy resin is:

- BDP 4294 (epoxy resin).
- CURAMINE 32-494 (curing agent).

The suggested cure schedule for this two-component system is 24 h at 25°C, followed by 1 h at 120°C and finally 2 more hours at 180°C. Compression modulus and strength of the cured resin have been determined experimentally and reported in literature.[29,30] All the experimental test campaign has been carried out on samples of the epoxy resin cured accordingly to the manufacturer's guidance. Moreover, five small cylindrical samples have been tested at room temperature to obtain compressive strength and modulus of the cured resin.

2.1.3 | Teflon

To produce the composite material panels for the fracture mechanics tests, it was necessary to insert two thin 13-μm-thick Teflon films at the ends of each panel between the layers of fabric before infusion. The introduction of the Teflon film was necessary to allow the future pre-cracking of the specimen as required by the reference standard (see Figure 1). The total thickness was between 6 and 8 mm.

2.1.4 | Panel manufacturing

The RTM instrument used vacuum to keep the lid closed. Full vacuum has been achieved on the flange and tool cavity. Numerous heating systems have been used to keep the resin and tool at the required temperatures. The press heating system used a proportional, integral,

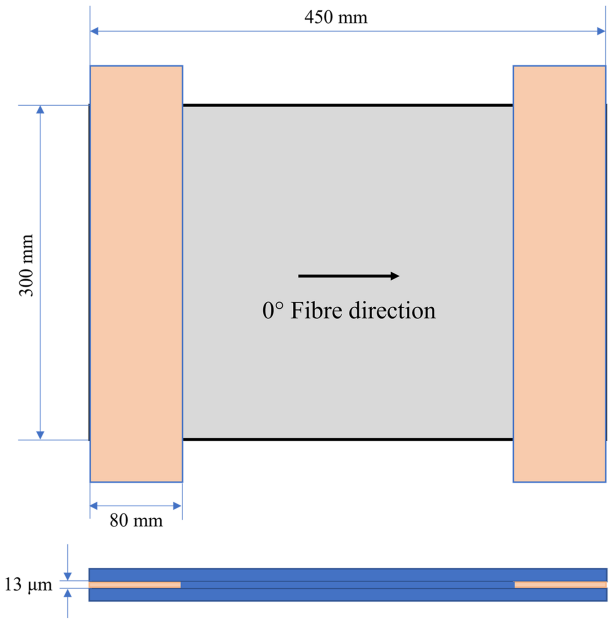

FIGURE 1 Panel to produce specimens for fracture mechanics tests. [Colour figure can be viewed at wileyonlinelibrary.com]

derivative (PID) controller and trace heater on the resin inlet tube. The oven used to preheat the resin also had a PID controller. The heating circuit on the mold used the main power of the press that comes from a three-phase 415-V socket. The compressor that supplies the pressurized air for resin injection also used a 415-V three-phase power outlet. Then, the epoxy and hardener have been preheated to 40°C. Once mixed, they have been placed in a heated pressure pot at 35°C. The tool surfaces have been heated to 35°C. The average time taken for the resin to fill the mold has been ∼105 min. Considering the UD panels, the filling has been achieved through a layup edge, which allowed the resin to travel along the length of the fibers. Full vacuum pressure and 1.0 bar injection pressure have been used. Teflon sheets have been held in their default position using both tape on the outside of the press and with the lid kept in the closed position.

2.2 | Standard test methods

The standard test methods used in this research are briefly summarized in this section.

- Mode I interlaminar fracture toughness of UD FRP matrix composites: ASTM D5528-13.
- Mode II interlaminar fracture for toughness of UD FRP composite: ASTM D7905M-14.
- Mixed Mode I–Mode II interlaminar fracture toughness of UD FRP composites: ASTM D6671M-06.
- Translaminar fracture toughness of laminated polymer matrix composite materials: ASTM E1922-97.

2.3 | Manufacturing strategy

All the coupons for the mechanical tests were obtained from composite panels having specific fiber layouts and thicknesses in accordance with the project plan. Two panels were used to derive the samples to be tested. The panel is composed by eight UD [0°] plies to extract specimens for Mode I, Mode II, Mixed Mode I–II, and translaminar fracture toughness tests, respectively.

2.4 | Manufacturing of coupons requirements and strategy

Coupons have been manufactured according to the quality standard required by the aeronautical sector when adopting RTM manufacturing processes to guarantee the maximum standard of quality while maintaining high level of repeatability. An overall amount of 30 specimens were tested. Eighteen samples were utilized to obtain the fracture toughness in Mode I, Mixed Mode I–II, and translaminar, whereas 12 samples were analyzed to determine the fracture toughness in Mode II.

2.5 | Test specimen production

Test specimens were extracted from composite panels using a Sharp & Tappin saw fitted with a metal-bonded diamond cutting disc. Then, they were machined to reach a 20 mm width. Areas to be bonded to hinges or blocks were accurately prepared by wet blasting using a Vapormatt vac blaster with 180–220 alumina grit, and this has allowed to achieve a water break free surface. After preparation, the surfaces were washed and dried. Surfaces were wiped with a solvent to remove any remaining contaminants before bonding. Blocks were glued to the Mode I specimens using a paste adhesive that was cured for 24 h at room temperature with contact pressure applied. Samples were then post cured at 65°C for 120 min.

2.6 | Specimen dimensions

The width and thickness of Mode I, Mixed Mode I–II, and translaminar fracture toughness specimen were measured at three different positions along the crack propagation path of each sample. The average values of these three measurements (both width and thickness) were

considered as the actual specimen dimensions during testing. The width of Mode II fracture toughness specimens was measured also in three different locations, whereas their thicknesses were measured at six dissimilar places along the crack propagation path. The average value of these measurements was assumed as actual dimension of the sample during testing. All dimensions were measured using calibrated digital calipers and micrometers.

2.7 | Test specimen

Experimental campaign has been performed using a Shimadzu AGS-X test machine fitted with a 10-kN load cell. The load cell is calibrated to BS EN ISO 7500-1:2018 and ASTM E4-20. Crack propagation monitoring was performed using an Imetrum Optical Video Gauge Crack Propagation Mode I Monitoring system using a Video Strain Gauge GP Lens, Calibrated to ISO9513 Class 0.5. The optical system works by using Imetrum crack growth software to track the growth of the crack by monitoring the displacement of multiple targets placed along the length of the specimen. The targets are made up from a pattern stamped onto the sides of the specimens, consisting of matt finish white paint that is sprayed onto the specimen edge and stamped with jet black ink 0.3-mm speckle diameter either side of the crack growth plane. The force and displacement data from the Shimadzu 10-kN test machine was outputted as a voltage and recorded alongside the raw data in the Imetrum System. The accuracy of the software tracking of the crack growth is visually confirmed on the recorded video. All mechanical testing was performed in a laboratory condition which are controlled to 23 ± 3°C and maximum of 60% RH. All RT specimens were left to stabilize for a minimum of 4 h at these conditions prior to testing.

3 | RESULTS AND DISCUSSION

Static tests were performed as required by the research project test plan. Experimental tests were accomplished in accordance with relevant standard test methods as described in the following sections.

3.1 | ASTM D5528: Mode I interlaminar fracture toughness

Mode I fracture toughness testing was performed using a double cantilever beam (DCB) specimen. After the Mode I fracture toughness specimens were machined, prepared, and labeled, the edges of the specimens were then sprayed with white paint. Loading blocks were positioned at the end of the specimens and bonded to the prepped surfaces of the specimen using a curing paste adhesive. After the crack had been initiated and grown to 50 mm in length, the tip of the crack was marked with a fine pencil. The specimens were then marked with a fine pencil at 1 mm intervals from the tip of the crack for the first 5 mm and then at 5 mm intervals up to 45 mm from the tip of the crack followed by 1 mm intervals from 45 to 50 mm (Figure 2).

3.1.1 | Mode I pre-cracking

Pre-cracking was executed at a constant crosshead speed of 2 mm/min until the crack is seen to grow by the recommended minimum of 3 mm from the insert, and the specimen was then unloaded.

3.1.2 | Mode I cracking

Crack propagation from the pre-crack was achieved at a crosshead speed of 2 mm/min until the crack had grown to a total length of greater than 50 mm from the end of the insert (see Figure 3).

3.1.3 | Mode I fracture toughness calculations

Although the pre-cracking and crack testing were in progress, the crack propagation was continuously monitored using the Imetrum Optical System. Load and displacement data from the Shimadzu 10-kN test machine were inputted into the Imetrum System. After testing was completed, the Imetrum Optical System raw data and test machine raw data were examined, and the load and displacement data for each crack propagation point noted. These loads, displacements, and crack lengths were then used to calculate the fracture toughness energies.

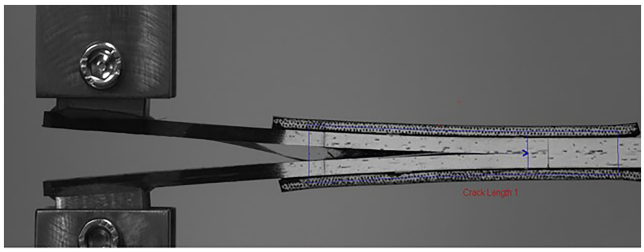

FIGURE 2 Mode I, DCB specimen during crack propagation [Colour figure can be viewed at wileyonlinelibrary.com]

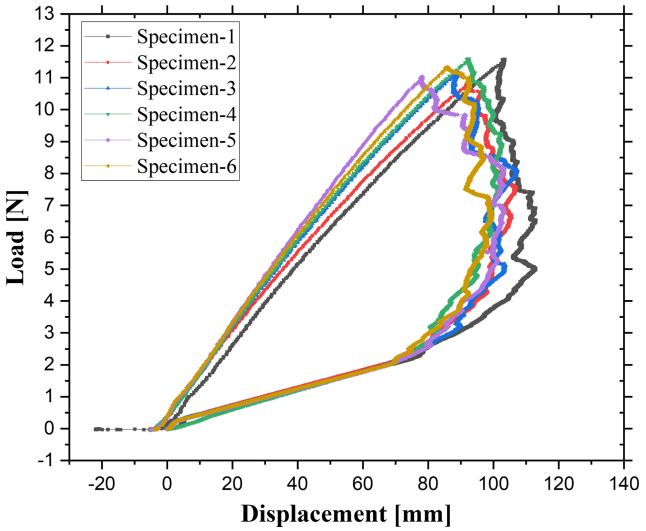

FIGURE 3 Mode I, crack propagation curves up to failure (raw data) [Colour figure can be viewed at wileyonlinelibrary.com]

Fracture toughness energies were calculated using the modified beam theory method MBT (Equation 1), namely, ASTM D5528 equation 7,

$$G_I = {}^{3P\delta}\!/_{2b(a+|\Delta|)} \quad (1)$$

compliance calibration method CC (Equation 2) (ASTM D5528 equation 9), and modified compliance calibration method MCC (Equation 3) (ASTM D5528 equation 10).

$$G_I = {}^{nP\delta}\!/_{2ba} \quad (2)$$

$$G_I = \left({}^{3P^2C^{2/3}}\right)\!/_{\left(2A_1bh\right)} \quad (3)$$

Fracture toughness energies were calculated for the nonlinear (NL), visual crack (VIS), 5% (if applicable), and maximum load (MAX) and for each of the crack propagation marks as the crack grew.

3.1.4 | Mode I fracture toughness

The results have been summarized in Table 1 as reported in that follows:

- Deviation from linearity (NL), visual observation (VIS), 5% offset (5%).
- Maximum load (MAX) for the actual cracking (AC) (not pre-cracking) of each Mode I specimen tested using the MBT, CC, and MCC methods and average Mode I fracture toughness for the crack propagation from 10 to 50 mm using the MBT, CC, and MCC methods of actual cracking (AC).

The following are the observed results for the 0° interface panels. The test results show average value for NL, VIS, 5%, and MAX were found to be 123.78, 126.91, 151.89, and 520.68 J/m^2, respectively. Their respective C of Vs were ∼8%, ∼8%, ∼7%, and ∼10%. The average fracture toughness for the crack propagation from 10 to 50 mm was 472.19 J/m^2 with C of V of ∼5%. Stable crack growth and fiber bridging were observed during testing. Failure occurred by the laminates stitching and by bridging of the UD fibers.

3.2 | ASTM D7905: Mode II interlaminar fracture toughness

Tests were carried out using end-notched flexure (ENF) specimen and fixture (see Figure 4). Exploratory specimens were cut and tested from each of the three materials to determine what compliance calibration loads to use to obtain the compliance calibration coefficients of the NPC and PC specimens for the different materials. The compliance calibration loads are used to determine the maximum load before unloading to obtain the compliance calibration coefficients, which is made more accurate by performing the exploratory tests of the specific material. The coefficients are then used to plot a graph of compliance (C) versus delamination cubed (a^3) to obtain the intercept (A), slope (m), and correlation coefficient of linear fit (r^2). Anyway, the recommended method by ASTM D7905 was to use a single specimen for both NPC (blunt cracking from the insert) and PC (sharp cracking) test. After the Mode II fracture toughness specimens were machined, prepared, and labeled, the end of the insert was located using an optical microscope, and its position marked on the specimen surface. The edges of the specimens were then sprayed with white paint. Specimens were then marked with a fine pencil at 20, 30, and 40 mm from the insert tip. After the NPC testing, the new tip of the crack was located and marked again at 20, 30, and 40 mm from the tip of the crack. The specimens are also marked with small pencil dots at 5 mm intervals to help to visually determine the crack length when using the Imetrum video camera.

3.2.1 | Mode II cracking

Crack propagation for NPC and PC tests was undertaken at a constant loading speed of 0.80 mm/min until movement of the crack and sufficient drop in load was observed; the specimen was then unloaded at a constant speed of 0.6 mm/min for NPC specimens and 1.6 mm/min for PC specimens. Testing was performed using

TABLE 1 Mode I, NL, VIS and 5% offset, maximum load, average propagation

Mode I: 0° interface									
Specimen ID	Nonlinear point (NL) Energy J/m²			Visual initiation (VIS) Energy J/m²			5% offset (5%) energy J/m²		
	MBT (Equation 7)	CC (Equation 9)	MCC (Equation 10)	MBT (Equation 7)	CC (Equation 9)	MCC (Equation 10)	MBT (Equation 7)	CC (Equation 9)	MCC (Equation 10)
Sp-1	115.2	123.9	113.4	115.24	123.9	113.4	159.83	169.4	159.84
Sp-2	135.1	144.8	134.36	142.19	152.4	141.24	143.57	152	144.01
Sp-3	125.2	134.3	122.82	125.19	134.3	122.82	155.99	165.8	154.08
Sp-4	115.6	126.3	115	115.58	126.3	115	153.18	166.3	152.23
Sp-5	135.2	144.8	133.63	135.4	145	133.69	163.84	174.2	162.94
Sp-6	116.4	126.3	115.4	127.88	138.8	126.84	134.93	145.4	134.21
Average	**123.8**	**133**	**122.44**	**126.91**	**137**	**125.5**	**151.9**	**162.2**	**151.2**
St. dev.	**9.54**	**9.51**	**9.53**	**10.71**	**10.9**	**10.78**	**10.78**	**11.06**	**10.6**
C of V	**7.71**	**7.13**	**7.78**	**8.44**	**8**	**8.59**	**7.1**	**6.82**	**7.01**

TABLE 1 (Continued)

Mode I: 0° interface									
Specimen ID	Maximum load fracture toughness (MAX) energy J/m²			Average propagation 10–50 mm (Prop) energy J/m²					
	MBT (Equation 7)	CC (Equation 9)	MCC (Equation 10)	MBT (Equation 7)	CC (Equation 9)	MCC (Equation 10)	C of V MBT	C of V CC	C of V MCC
Sp-1	496.75	476.1	511.3	495.2	464.91	499.07	25.95	22.73	25.22
Sp-2	520.58	492.1	531.58	458.8	430.52	462.42	27.64	24.6	26.96
Sp-3	591.82	566.7	600.9	493.6	470.83	495.72	23.1	20.47	22.8
Sp-4	566.09	533.5	568.25	480.1	453.96	480.87	29.21	26.1	28.95
Sp-5	509.37	494.5	522.89	469.4	448.01	471.97	20.53	18.39	20.29
Sp-6	439.49	420.2	450.77	436.1	410.43	438.43	28.04	24.79	27.46
Average	**520.7**	**497.2**	**530.95**	**472**	**446.4**	**474.8**			
St. dev.	**53.69**	**50.09**	**51.31**	**22.5**	**22.56**	**22.57**			
C of V	**10.31**	**10.08**	**9.66**	**4.77**	**5.05**	**4.75**			

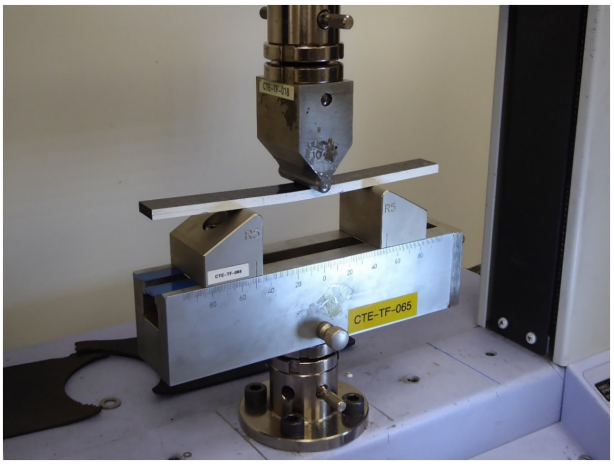

FIGURE 4 Mode II, ENF specimen while loaded. [Colour figure can be viewed at wileyonlinelibrary.com]

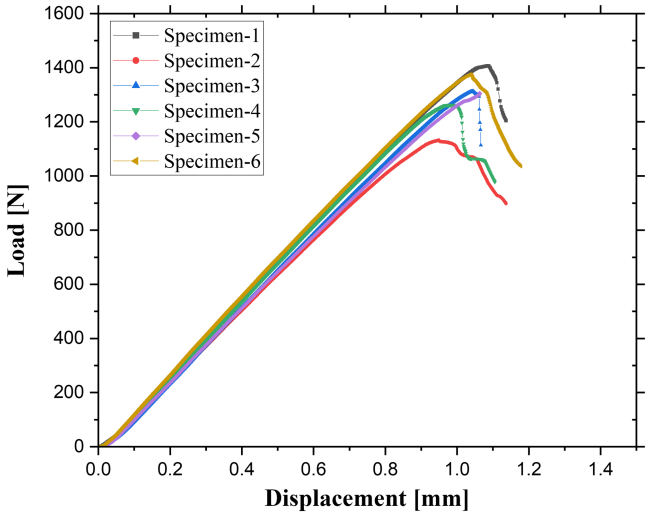

FIGURE 5 Mode II, crack propagation curves up to failure (raw data) [Colour figure can be viewed at wileyonlinelibrary.com]

10-mm-diameter loading noses and supports with a fixed span of 100 mm. Raw data of crack propagation curves have been shown in Figure 5.

3.2.2 | Mode II fracture toughness calculations

While testing was in progress, the crack propagation was continuously recorded using the Imetrum video camera. The recording is purely for the purpose of visual determination of where the crack tip ends. Fracture toughness energies were calculated using the CC method as detailed in ASTM D7905. The compliance calibration coefficients are plotted on a graph to determine the slope and the intercept of the curve fit of the C versus a^3 data. The slope, unloading compliance, maximum load, and specimen width were used to calculate the candidate toughness. The peak percentage of the candidate toughness is calculated to determine if candidate toughness = fracture toughness. If the peak percentage of the candidate toughness is within 15%–35%, then the candidate toughness is equal to the Mode II fracture toughness.

3.2.3 | Mode II fracture toughness

The G_{IIC} CC is valued from tested using Equations (4)–(6), ASTM D7905 equations (3), (4), and (6), for both NPC and PC specimens.

$$G_Q = \left(3mP_{Max}^2 a_0^2\right)/2B \tag{4}$$

$$G_Q = \left(3mP_{Max}^2 a_{PC}^2\right)/2B \tag{5}$$

$$\%G_{Q,j} = \left[\left(100P_j a_j\right)^2/\left(P_{Max} a_0\right)^2\right]; j = 1,2 \tag{6}$$

The following are the observed results for the 0° interface panels. The average fracture toughness for the NPC compliance calibration G_{IIC} value was 866.27 J/m^2 with C of V of ~7%. The average fracture toughness for the PC compliance calibration G_{IIC} value was 748.26 J/m^2 with C of V of ~14%. It should be noted that a test error has occurred of which the compliance calibration load for 20 mm has been used for 40 mm and vice versa but was deemed irrelevant due to the graph's linear properties in relation to the compliance. All results were reported in Tables 2 and 3.

3.3 | ASTM D6671: Mixed Mode I–II Interlaminar fracture toughness

Mixed Mode I–II fracture toughness testing was carried out using a mixed mode bending apparatus (see Figure 4). The mode mixture G_{II}/G for the test is 0.5. After the specimens were machined, prepared, and labeled, the end of the insert was located using an optical microscope, and its position marked on the specimen surface. The edges of the specimens were then sprayed with white paint. The Mixed Mode I–II fracture toughness specimens were then marked with pencil at 1 mm intervals from the end of the insert for the first 5 mm and then at 5 mm intervals up to 25 mm. Piano Hinges were positioned 25 mm from the end of the insert and bonded to the surfaces of the specimens using a curing paste adhesive (see Figure 6).

TABLE 2 Mode II, NPC CC loads and compliances, NPC fracture toughness

Mode II: 0° interface NPC														
	CC loads (N)		**Compliances (mm/N)**											
Specimen	**At a_1 (mm)**	**At a_2 (mm)**	**C(a_1)**	**C(a_2)**	**C (a_o)**	**A**	**m**	**r^2**	**P_{max} (N)**	**G_Q (J/m^2)**	**%G_Q ($a = a_1$)**	**%G_Q ($a = a_2$)**	**G_{IIc} (J/m^2)**	**a_{calc} (mm)**
Sp-1	1056.34	528.17	0.00056	0.00093	0.0007	5.14E-07	0.0066	0.998	1366.03	822.33	26.58	26.58	822.33	36.02
Sp-2	1020.25	510.12	0.00058	0.00099	0.00074	5.31E-07	0.0072	0.997	1275.75	792.79	28.42	28.42	792.79	43.08
Sp-3	1086.91	543.46	0.00056	0.00094	0.0007	5.11E-07	0.0067	0.999	1381.49	866.01	27.51	27.51	866.01	39.93
Sp-4	1115.99	557.99	0.00057	0.00094	0.00071	5.24E-07	0.0066	0.998	1457.14	935.06	26.07	26.07	935.06	44.72
Sp-5	1113.88	556.94	0.00058	0.00095	0.00071	5.29E-07	0.0066	1	1457.82	942	25.95	25.95	942	40.9
Sp-6	1072.29	536.14	0.00056	0.00093	0.00069	5.09E-07	0.0066	1	1376.61	839.41	26.97	26.97	839.41	43.98
Average	**1077.61**	**538.8**	**0.0006**	**0.001**	**0.0007**	**5.20E-07**	**0.007**	**0.999**	**1385.8**	**866.27**	**26.92**	**26.92**	**866.27**	**41.44**
St. dev.	**36.46**	**18.23**	**1E-05**	**2E-05**	**2E-05**	**9.58E-09**	**3E-04**	**0.001**	**67.65**	**60.86**	**0.94**	**0.94**	**60.86**	**3.22**
C of V (%)	**3.38**	**3.38**	**1.73**	**2.38**	**2.43**	**1.84E+00**	**4.02**	**0.12**	**4.88**	**7.03**	**3.49**	**3.49**	**7.03**	**7.78**

TABLE 3 Mode II, PC CC loads and compliances, PC fracture toughness

Mode II: 0° interface PC														
	CC loads (N)		**Compliances (mm/N)**											
Specimen	**At a_1 (mm)**	**At a_2 (mm)**	**C(a_1)**	**C(a_2)**	**C (a_o)**	**A**	**m**	**r^2**	**P_{max} (N)**	**G_Q (J/m^2)**	**%G_Q (a = a_1)**	**%G_Q (a = a_2)**	**G_{IIc} (J/m^2)**	**a_{calc} (mm)**
Sp-1	1087.99	544	0.0006	0.0009	0.0007	5.14E-07	0.007	0.998	1407	872.34	26.58	26.58	872.34	42.31
Sp-2	876.68	438.34	0.0006	0.001	0.0008	5.48E-07	0.007	0.991	1132.2	604.7	26.65	26.65	604.7	41.78
Sp-3	1043.54	521.77	0.0006	0.001	0.0007	5.12E-07	0.007	0.997	1313.5	800.74	28.05	28.05	800.74	43.75
Sp-4	922.43	461.22	0.0006	0.0009	0.0007	5.28E-07	0.006	0.998	1262.2	644.16	23.74	23.74	644.16	44.27
Sp-5	994.94	497.47	0.0006	0.001	0.0007	5.45E-07	0.007	0.996	1310.3	774.47	25.63	25.63	774.47	41.65
Sp-6	1040.89	520.45	0.0006	0.0009	0.0007	5.11E-07	0.006	1	1374.6	793.14	25.48	25.48	793.14	41.28
Average	**994.41**	**497.21**	**0.0006**	**0.0009**	**0.0007**	**5.26E-07**	**0.007**	**0.997**	**1299.9**	**748.26**	**26.02**	**26.02**	**748.26**	**42.51**
St. dev.	**80.46**	**40.23**	**1E-05**	**3E-05**	**3E-05**	**1.71E-08**	**4E-04**	**0.003**	**96.85**	**102.27**	**1.45**	**1.45**	**102.27**	**1.22**
C of V (%)	**8.09**	**8.09**	**2.57**	**3.46**	**4.13**	**3.24E+00**	**5.84**	**0.32**	**7.45**	**13.67**	**5.57**	**5.57**	**13.67**	**2.87**

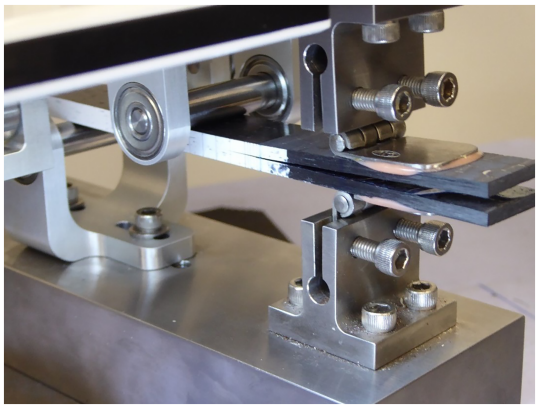

FIGURE 6 Mixed mode I-II, details of tested specimen. [Colour figure can be viewed at wileyonlinelibrary.com]

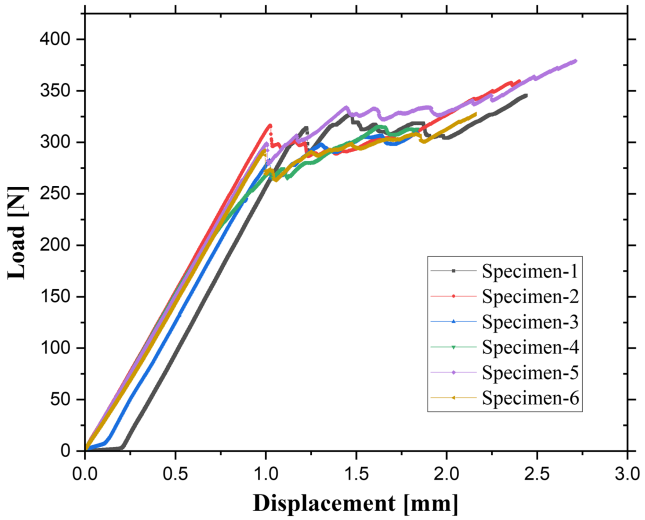

FIGURE 7 Mixed Mode I–II, crack propagation curves up to failure (raw data) [Colour figure can be viewed at wileyonlinelibrary.com]

3.3.1 | Preliminary data

All preliminary data needed are taken from the other tests, that is, longitudinal tensile modulus are taken from the 0° tensile test results with their respective test conditions. An exception was G_{13} out-of-plane shear modulus where G_{12} shear modulus from the in-plane shear test was used instead as suggested by the standard in ASTM D6671 section 12.1, "The preceding equations calls for the out-of-plane shear modulus, G_{13}, which may be assumed equal to the in-plane shear modulus, G_{12}, for unidirectional composite."

3.3.2 | Mixed Mode I–II cracking

Crack propagation was implemented at a crosshead speed of 1 mm/min until the crack reached a total length greater than 25 mm from the end of the insert. Raw data of crack propagation are shown in Figure 7.

3.3.3 | Mixed Mode I–II fracture toughness calculations

While the crack testing was in progress, the crack propagation was continuously monitored using the Imetrum Optical System. Load and displacement data from the Shimadzu 10-kN test machine were inputted into the Imetrum System (see Figure 8). After testing was completed, the Imetrum Optical System raw data and test machine raw data were examined, and the load and displacement data for each crack propagation point noted. These loads, displacements, and crack lengths were then used to calculate the fracture toughness energies.

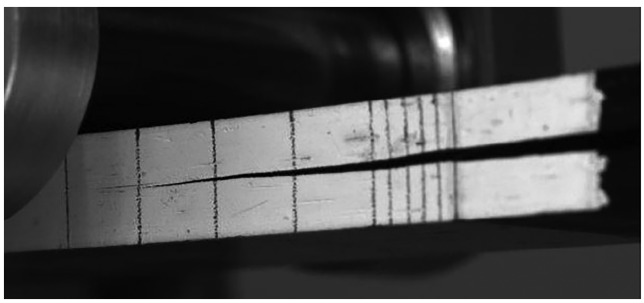

FIGURE 8 Mixed Mode I–II failure

Fracture toughness energies were calculated using Equations (7)–(10), namely, using ASTM D6671 equations (12)–(15).

$$G_I = \left[12P^2(3c-L)^2/16b^2h^3L^2E_{1f}\right](a+\chi h)^2 \tag{7}$$

$$G_{II} = \left[9P^2(c+L)^2/16b^2h^3L^2E_{1f}\right](a+0.42\chi h)^2 \tag{8}$$

$$G = G_I + G_{II} \tag{9}$$

$$G_{II}/G = G_{II}/(G_I+G_{II}) \tag{10}$$

Fracture toughness energies were calculated for the NL, MAX, 5% (if applicable), and VIS points and for each of the crack propagation marks as the crack grew. When 3% of critical load (MAX) is below than the lever weight, Lever Weight Corrections must be applied to the whole

TABLE 4 Mixed Mode I-II, NL, VIS and 5% offset, average propagation

Mixed Mode I–II: 0° interface									
	Nonlinear point (NL) energy J/m^2				Visual initiation (VIS) energy J/m^2				5% offset (5%) energy J/m^2
Specimen ID	**G_I**	**G_{II}**	**G_c**	**G_{II}/G (%)**	**G_I**	**G_{II}**	**G_c**	**G_{II}/G (%)**	**G_I**
Sp-1	75.35	88.19	163.5	53.93	93.68	110.6	204.26	54.14	93.67
Sp-2	91.29	106.8	198.1	53.92	98.45	116.2	214.66	54.14	91.24
Sp-3	65.49	76.65	142.1	53.93	65.49	76.65	142.13	53.93	78
Sp-4	33.16	38.81	71.97	53.93	72.01	84.29	156.29	53.93	-
Sp-5	70.1	82.04	152.1	53.92	87.42	102.3	189.74	53.92	88.88
Sp-6	75.52	88.4	163.9	53.93	75.52	88.4	163.92	53.93	101.2
Average	**68.5**	**80.16**	**148.6**	**53.9**	**82.1**	**96.41**	**178.5**	**54**	**90.6**
St. Dev.	**19.4**	**22.67**	**42.04**	**0**	**13**	**15.68**	**28.72**	**0.11**	**8.43**
C of V	**28.3**	**28.28**	**28.29**	**0**	**15.9**	**16.27**	**16.09**	**0.2**	**9.31**

TABLE 4 (Continued)

Mixed Mode I–II: 0° interface											
	5% offset (5%) energy J/m^2			Average propagation from 10 to 25 mm							
Specimen ID	**G_{II}**	**G_c**	**G_{II}/G (%)**	**G_I**	**G_{II}**	**G_c**	**G_{II}/G (%)**	**C of V G_I**	**C of V G_{II}**	**C of V G_c**	**C of V G_{II}/G (%)**
Sp-1	110.6	204.25	54.14	220	284.49	504.49	56.29	23.45	25.67	24.7	1.02
Sp-2	107.7	198.94	54.14	235.7	305.96	541.65	56.28	51.75	53.93	52.98	1.02
Sp-3	92.82	170.82	54.34	199.8	258.68	458.48	56.29	30.26	32.33	31.43	1.02
Sp-4	-	-	-	264.8	343.44	608.25	56.29	41.36	43.52	42.58	1.02
Sp-5	104.9	193.8	54.14	280.4	363.47	643.9	56.29	39.76	41.97	41.01	1.02
Sp-6	122.2	223.46	54.7	215.8	279.71	495.49	56.29	38.02	40.18	39.24	1.02
Average	**108**	**198.3**	**54.29**	**236.1**	**305.96**	**542**	**56.29**				
St. Dev.	**10.6**	**19**	**0.25**	**30.92**	**40.24**	**71.16**	**0**				
C of V	**9.84**	**9.58**	**0.45**	**13.1**	**13.15**	**13.13**	**0**				

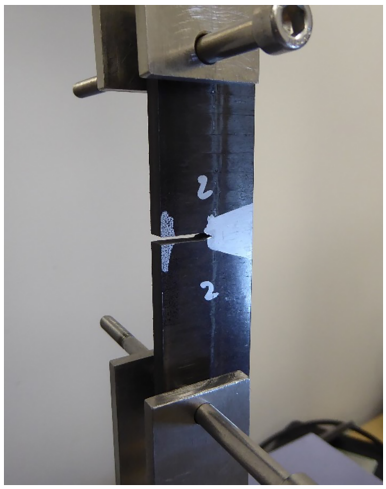

FIGURE 9 View of the specimen before the translaminar fracture toughness test [Colour figure can be viewed at wileyonlinelibrary.com]

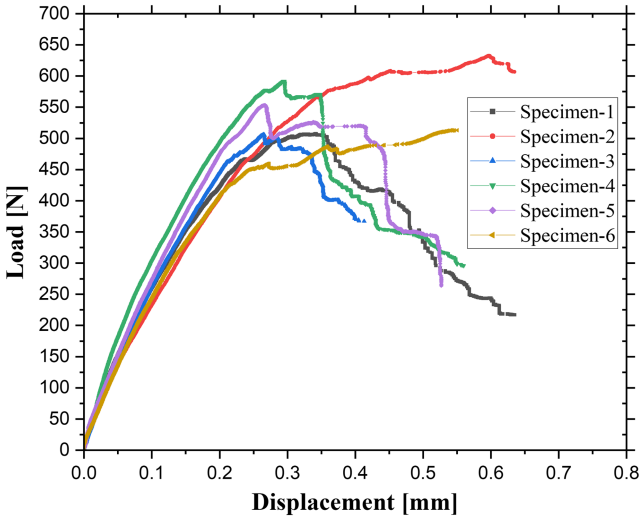

FIGURE 10 Translaminar crack propagation curves up to failure (raw data) [Colour figure can be viewed at wileyonlinelibrary.com]

batch. Fracture toughness energies were then calculated using the ASTM D6671 equations (17)–(19). All batch tested were corrected.

3.3.4 | Mixed Mode I–II fracture toughness

The results can be summarized as follows:

- Visual observation (VIS) and maximum load (MAX) for the actual cracking (AC) (not pre-cracking) of each Mixed Mode I–II specimen tested using the ASTM D6671 equation 12 for G_I, equation 13 for G_{II}, equation 14 for the total mixed mode strain energy release rate G, equation 15 for the mode mixture G_{II}/G, and equation 16 (Equation 11) for mixed mode fracture toughness Gc.

$$G_c = G|_{P_c, a_0} \tag{11}$$

- Most 5% data were not included due to C5% (5% of compliance) condition was found to occur before the VIS point or after MAX on some specimen.
- Average Mixed Mode I–II fracture toughness for the crack propagation from 1 to 25 mm have been calculated using the ASTM D6671 equations 12–14.
- If the 3% of critical applies load P3% is lower than the lever weight Pg, the whole batch will be subjected to lever weight corrections calculation using Equations (12)–(14), ASTM D6671 equations 17–19, respectively.

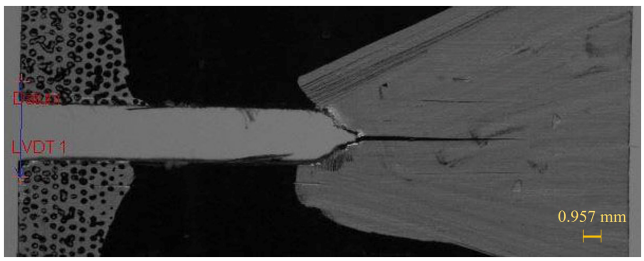

FIGURE 11 Translaminar fracture toughness test during crack propagation [Colour figure can be viewed at wileyonlinelibrary.com]

$$G_I = \left\{12\left[\left(P(3c-L)+P_g\left(3c_g-L\right)/\right]^2/\left(16b^2h^3L^2E_{1f}\right)\right\}(a+\chi h)^2 \tag{12}$$

$$G_{II} = \left\{9\left[P(c+L)+P_g\left(c_g+L\right)\right]^2/\left(16b^2h^3L^2E_{1f}\right)\right\}(a+0.42\chi h)^2 \tag{13}$$

$$c = \left(1+P_g/P_c\right)\left[\left(12\beta^2+3\alpha+8\sqrt{3\alpha}\right)/\left(36\beta^2-3\alpha\right)\right]L - P_g/P_c c_g \tag{14}$$

It is worth noting that the fracture toughness energies discussed below are the values calculated using the Equation (11) G_c with lever weight corrections as it gives more correct mode mixture that was intended. Observed results for the 0° interface panels have been reported in that follows. The test results show average value for NL, VIS, 5%, and MAX were found to be 148.64, 178.50, 198.26, and 762.99 J/m^2, respectively. Their respective C of Vs were ~28%, ~16%, ~10%, and ~34%. The average fracture toughness for the crack propagation from 10 to 25 mm was 542.04 J/m^2 with C of V of ~13%. Secondaries

TABLE 5 Translaminar fracture toughness 90° interface, initial configuration of specimens, slope chord, load intercept, K_{TL} criterion

Translaminar 90° interface						Slope chord				
						Preset 1		Preset 2		Gradient
Specimen ID	Width [W] (mm)	Thickness [B] (mm)	Notch length [a] (mm)	Max Force [P_{max}] (N)	Notch-mouth displacement [V_{max}] mm	Force (N)	Notch disp. (mm)	Force (N)	Notch Disp. (mm)	(N/mm)
Spec-1	30.08	6.17	15.9	507.4	0.34	50	0.0128	150	0.0487	2784.74
Spec-2	29.99	6.12	16.03	632.74	0.37	50	0.0169	150	0.0553	2606.88
Spec-3	30.05	6.18	15.64	506.83	0.32	50	0.0164	150	0.0537	2678.81
Spec-4	30.03	6.13	15.83	591.93	0.29	50	0.0116	150	0.0452	2969.12
Spec-5	30.02	6.2	15.66	553.3	0.27	50	0.0156	150	0.0508	2848.19
Spec-6	30.02	6.15	16.84	518.04	0.46	50	0.0192	150	0.0619	2341.92
Average	**30.03**	**6.16**	**15.98**	**551.71**	**0.34**					
St. dev.	**0.03**	**0.03**	**0.44**	**51.57**	**0.07**					
C of V (%)	**0.1**	**0.5**	**2.78**	**9.35**	**20.35**					

TABLE 5 (Continued)

Translaminar 90° interface	Load intercept			Intermediate calculations			Notch length Criteria	K_{TL} criterion	
Specimen ID	(N)	V_{n-0}	ΔV_n	Width (m)	Thickness (m)	Force (MN)	0.5 W < an <0.6 W	$\Delta V_n/V_{n-0 \leq 0.3}$	K_{TL} (MPa·$m^{1/2}$)
Spec-1	14.27	0.18	0.16	0.301	0.0617	0.000507	0.53	0.93	115.58
Spec-2	5.94	0.24	0.12	0.3	0.0612	0.000633	0.53	0.52	148.84
Spec-3	6.15	0.19	0.13	0.301	0.0618	0.000507	0.52	0.69	111.86
Spec-4	15.68	0.19	0.09	0.3	0.0613	0.000592	0.53	0.47	135.09
Spec-5	5.45	0.19	0.08	0.3	0.062	0.000553	0.52	0.42	122.32
Spec-6	5.11	0.22	0.25	0.3	0.0615	0.000518	0.56	1.12	134.35
Average								**Average**	**128.01**
St. dev.								**St. Dev.**	**13.94**
C of V (%)								**C of V (%)**	**10.89**

crack propagation observed from probable 20-mm growth, which increase the load, thus making the max load higher. Specimens 1 and 3 shows less fiber bridging—thus a lower max load. Mixed Mode I–II testing is initially predominantly Mode I at start and then transition into Mode II as it bends. The load–displacement graphs support this as low load at the start of the crack propagation going to high load at the end, which is typical of Mode II. Thus, as a system, the average propagation was taken between 10 and 25 mm to correspond to the results of the Mode I and Mode II. All results were reported in Table 4.

3.4 | ASTM E1922: Translaminar fracture toughness

Testing was completed using eccentrically loaded single-edge-notch specimen. The notch width was made with 2-mm band saw about 5 mm first and then continued to be sawed with 0.1-mm knife edge (see Figure 9).

3.4.1 | Translaminar fracture toughness cracking

Crack propagation was performed at a crosshead speed of 0.5 mm/min until the crack had grown and a definite load drop from the max load (see Figure 10).

3.4.2 | Translaminar fracture toughness calculations

While the crack testing was in progress, the crack propagation was continuously monitored using the Imetrum Optical System to measure the notch displacement V_n and inputted into the Shimadzu 10-kN test machine (see Figure 11). After testing was completed, the load for each notch-displacement points were noted, and two preset load force are picked for the slope to calculate ΔV_n and V_n-0. These loads and notch-displacement were then used to calculate the applied stress intensity factor. The applied stress intensity factor were calculated using the ASTM E1922 equation 1 (Equation 15).

$$K = \left[P/BW^{1/2}\right]\alpha_1^{1/2}\left[1.4+\alpha_1\right]\left[\begin{array}{l}3.97-10.88\alpha_1+26.25{\alpha_1}^2-38.9{\alpha_1}^3\\+30.15{\alpha_1}^4-9.27{\alpha_1}^5\end{array}\right] \Big/ \left[1-\alpha_1\right]^{3/2} \quad (15)$$

Then, the K_{TL} translaminar has been valued from ASTM E1922 equation 1 (Equation 15) following the procedure indicated in point 9.3 of ASTM E1922. Specimen has been tested using the ASTM D6671 equation 12 (Equation 7) for G_I, equation 13 (Equation 8) for G_{II}, equation 14 (Equation 9) for the total mixed mode strain energy release rate G, equation 15 (Equation 10) for the mode mixture G_{II}/G, and equation 16 (Equation 11) for mixed mode fracture toughness G_c.

3.4.3 | Translaminar 90° interface

Observed results for the 90° interface panels have been reported in that follows (Table 5). The average translaminar fracture toughness were found to be 128.01 MPa·$m^{1/2}$ with C of V of ∼11%. During testing, the specimens were observed to either have mainly stable crack growth or mixed with crack growth going through the stitching. All specimens did not pass the K_{TL} criterion of $\Delta Vn/Vn\text{-}0 \leq 0.3$. In author's opinion and experiences with crack growth propagation, the material needed to be stiffer in the 90°, which can only be achieved by a more brittle resin to absorb more energy before the crack propagates for it to pass the criterion. The specimen direction of 90° UD only has the resin to rely on for its stiffness during test. The standard's ASTM Task Group used a quasi-isotropic [90/−45/0/+45]4S carbon for their interlaboratory test program. The quasi-isotropic will have more stiffness perpendicular to the crack growth. The specimen direction of 0° UD is not the ideal material configuration; crack growth usually follows the 0° direction of the fiber between plies; thus, on a 0° specimen, the crack growth will only go up instead of the intended plane as shown by the preliminary test conducted; hence, the 90° UD direction was used to be able to propagate through the notch.

4 | CONCLUSIONS

The NCF composite material for aerospace use has been designed and produced to be reliable and therefore ensure the necessary resistance to fracture in operating conditions. Understanding the reliability of a structural component is very important to ensure that the final product will meet all the requirements of its intended use. The reliability of a composite structural component can be known through several experimental tests able to calculate its fracture toughness. These tests were carried out and shown in this work. The materials constituting the NCF composite for the aerospace sector were identified, and its mechanical behavior under different load conditions has been already evaluated in previous works both at room temperature and at high and low temperature. The evaluation of the mechanical properties obtained with different temperatures showed that this

new composite material can be used in the aeronautical sector. However, the fracture toughness evaluated in different test conditions must be carefully considered because it introduces limits on the use of this composite material. The results of these tests show that overall, the NCF composite material has good fracture toughness. However, the fracture toughness values of the translaminar should be increased. In the latter case, one way to increase the fracture toughness can be to increase the toughness of the resin or the use of through-thickness reinforcement by stitching. Effectively, the K_{TL} criterion showed somewhat low values compared with those expected for this type of composite material. Therefore, increasing the stiffness in the 90° would be appropriate and as indicated above, and, this result can be obtained by using a more brittle resin to absorb more energy before the crack propagates.

ACKNOWLEDGMENTS

This project has received funding from the Clean Sky 2 Joint Undertaking (JU) under grant agreement No 831955. The JU receives support from the European Union's Horizon 2020 research and innovation programme and the Clean Sky 2 JU members other than the Union.

DATA AVAILABILITY STATEMENT

The data that support the findings of this study are available from the corresponding author upon reasonable request.

NOMENCLATURE

ASTM	American Society for Testing and Materials
AC	actual cracking
A_1	slope of plot of a/b versus $C^{1/3}$
a,a_0	delamination length
a_j	the *j*th crack length used during compliance calibration
a_{pc}	actual crack length
b	specimen width
c	lever length of the test apparatus
c_g	lever length to center of gravity
B	specimen thickness
C	compliance of specimen
CC	compliance calibration
C of V	coefficient of variance
DCB	double cantilever beam
ENF	end-notched flexure
E_{1f}	modulus of elasticity in the fiber direction measured in flexure
G	energy release rate
G_c	critical energy release rate
G_{Ic}	G_c of Mode I
G_{IIc}	G_c of Mode II
G_{II}/G	mode mixture
G_Q	candidate Mode II interlaminar fracture toughness
h	thickness or half-thickness of specimen
K	applied stress intensity factor
K_{TL}	translaminar fracture toughness criterion
L	specimen half-span
MAX	maximum load
MBT	modified beam theory
MCC	modified compliance calibration
m	slope of compliance
NCF	non-crimp fabric
NL	nonlinear
NPC	non-pre-cracked
P	applied load
P_c	critical load
PID	proportional, integral, derivative
P_{Max}, P_g	weight of lever and attach apparatus (N)
PC	maximum value of force applied pre-cracked
QU	quasi-unidirectional
RH	relative humidity
RTM	resin transfer molding
RT	room temperature
Tg	glass transition temperature
5%C	5% compliance
$\%G_Q$	peak percentage of G_Q
VIS	visual inspection
V_n	notch-mouth displacement
$V_{n\text{-}o}$	V_n at maximum load
W	specimen width
α	mode mixture transformation parameter for setting lever length
α_1	dimensionless ratio a/W
β	nondimensional crack length correction for mode mixture
χ	crack length correction parameter
δ	load point deflection
Δ	effective delamination extension
ΔV_n	additional notch-mouth displacement>

REFERENCES

1. Lomov SV. *Non-crimped fabric composites*. 1st ed. Woodhead Publishing; 2011.
2. Veldenz L, Di Francesco M, Giddings P, Kim BC, Potter K. Material selection for automated dry fibre placement using the analytical hierarchy process. *Adv Manuf Polym Compos Sci*. 2018;4:83-96.

3. Mikhaluk DS, Truong TC, Borovkov AI, Lomov SV, Verpoest I. Experimental observations and finite element modelling of damage and fracture in carbon/epoxy non-crimped fabric composites. *Eng Fract Mech*. 2008;75(9):2751-2766.
4. Saito H, Kimpara I. Evaluation of impact damage mechanism of multi-axial stitched CFRP laminate. *Compos - A: Appl Sci Manuf*. 2006;37(12):2226-2235.
5. Bibo GA, Hogg PJ, Kemp M. Mechanical characterisation of glass- and carbon-fibre-reinforced composites made with non-crimped fabrics. *Comp Sci Techn*. 1997;57(9-10):1221-1241.
6. Talreja R. A continuum mechanics characterization of damage in composite materials. *Proc R Soc Lond*. 1985;A399(1817): 195-216.
7. Allen DH, Harris CE, Groves SE. Damage modeling in laminated composites. In: Boehler JP, ed. *Yielding, damage, and failure of anisotropic solids*. London: Mechanical Engineering Publications; 1990:535-550.
8. Edgren F, Mattsson D, Asp LE, Varna J. Formation of damage and its effects on Non-crimped fabric reinforced composites loaded in tension. *Compos Sci Technol*. 2004;64:675-692.
9. Nonn S, Kralovec C, Schagerl M. Damage mechanisms under static and fatigue loading at locally compacted regions in a high pressure resin transfer molded carbon fibre Non-crimped fabric. *Compos Part A Appl Sci Manuf*. 2018;115:57-65.
10. Smith P, Rudd CD, Long AC. The effect of shear deformation on the processing and mechanical propertis of aligned reinforcement. *Compos Sci Technol*. 1997;57(3):327-284.
11. Shipsha A, Burman M. Failure mechanisms in NCF composite bolted joints: experiments and FE model. *Compos Part B Eng*. 2020;192:107950.
12. Shipsha A, Hallström S, Burman M. Effect of stacking sequence and bundle waviness in quasi-isotropic NCF composites subjected to compression. *Compos Part B Eng*. 2019;178:107423.
13. Wilhelmsson D, Gutkin R, Edgren F, Asp LE. An experimental study of fibre waviness and its effects on compressive properties of unidirectional NCF composites. *Compos Part A Appl Sci Manuf*. 2018;107:665-674.
14. Edgren F, Asp LE, Joffe R. Failure of NCF composites subjected to combined compression and shear loading. *Compos Sci Technol*. 2006;66(15):2865-2877.
15. Vallons K, Duque I, Lomov SV, Verpoest I. Loading direction dependence of the tensile stiffness, strength and fatigue life of biaxial carbon/epoxy NCF composites. *Compos Part A Appl Sci Manuf*. 2011;42(1):16-21.
16. de Verdiere MC, Skordos AA, May M, Walton AC. Influence of loading rate on the delamination response of untufted and tufted carbon epoxy non crimp fabric composites: mode I. *Eng Fract Mech*. 2012;96:11-25.
17. Blackman BRK, Brunner AJ, Williams JG. Mode II fracture testing of composites: a new look at an old problem. *Eng Fract Mech*. 2006;73(16):2443-2455.
18. Park SJ, Kim MH, Lee JR, Choi S. Effect of fiber–polymer interactions on fracture toughness behavior of carbon fiber-reinforced epoxy matrix composites. *J Colloid Interface Sci*. 2000;228(2):287-291.
19. Fernández MV, de Moura MFSF, da Silva LFM, Marques AT. Mixed-mode I + II fatigue/fracture characterization of composite bonded joints using the single-leg bending test. *Compos A: Appl Sci Manuf*. 2013;44:63-69.
20. Kenane M, Benzeggagh ML. Mixed-mode delamination fracture toughness of unidirectional glass/epoxy composites under fatigue loading. *Compos Sci Technol*. 1997;57(5):597-605.
21. Carlsson LA, Gillespie JW Jr, Pipes RB. On the analysis and design of the end notched flexure (ENF) specimen for mode II testing. *J Compos Mater*. 1986;20(6):594-604.
22. Joshi A, Gouda PS, Sridhgar I, et al. Crack suppression by natural fiber integration for improved interlaminar fracture toughness in fiber hybrid composites. *Frat Integrita Strutt*. 2022; 16(60):158-173.
23. Ravandi M, Teo WS, Yong MS, Tay TE. Prediction of mode I interlaminar fracture toughness of stitched flax fiber composites. *J Mater Sci*. 2018;53(6):4173-4188.
24. Cui WC, Wisnom MR, Jones M. A comparison of failure criteria to predict delamination of unidirectional glass/epoxy specimens waisted through the thickness. *Composites*. 1992; 23(3):158-166.
25. Chen X, Sun X, Chen P, Chai Y. A delamination failure criterion considering the effects of through-thickness compression on the interlaminar shear failure of composite laminates. *Compos Struct*. 2020;241:112121.
26. Camanho PP, Davila CG, De Moura MF. Numerical simulation of mixed-mode progressive delamination in composite materials. *J Compos Mater*. 2003;37(16):1415-1438.
27. Molker H, Gutkin R, Asp LE. Implementation of failure criteria for transverse failure of orthotropic Non-Crimp Fabric composite materials. *Compos A: Appl Sci Manuf*. 2017;92:158-166.
28. Molker H, Wilhelmsson D, Gutkin R, Asp LE. Orthotropic criteria for transverse failure of non-crimp fabric-reinforced composites. *J Compos Mater*. 2016;50(18):2445-2458.
29. Lepore MA, Ferrante L, Sanguigno L, Maligno AR. A non-crimped fabric mechanical characterization for the production of aerospace components. *Mater Des Process Comm (MDPC)*. 2021;3(5):e222. doi:10.1002/mdp2.222
30. Lepore MA, Maligno AR, Harris L. Effects of temperature in novel crimp-free based composite materials for aerospace applications: an experimental assessment. *Compos Part C: Open Access*. 2021;6:100202.
31. Wang K, Young B, Smith ST. Mechanical properties of pultruded carbon fibre-reinforced polymer (CFRP) plates at elevated temperatures. *Eng Struct*. 2011;33(7):2154-2161.
32. Yu B, Kodur V. Effect of temperature on strength and stiffness properties of near-surface mounted FRP reinforcement. *Compos Part B Eng*. 2014;58:510-517.
33. Jia Z, Li T, Chiang F-P, Wang L. An experimental investigation of the temperature effect on the mechanics of carbon fiber reinforced polymer composites. *Compos Sci Technol*. 2018;154: 53-63.